mater.scichina.com link.springer.com

Published online 19 July 2022 | https://doi.org/10.1007/s40843-022-2101-2
Sci China Mater 2022, 65(11): 2967–2974

Interface engineering by gelling sulfolane for durable and safe Li/$LiCoO_2$ batteries in wide temperature range

Xinrun Yu and Xianluo Hu*

ABSTRACT **Lithium-metal batteries (LMBs) with high energy densities have aroused intensive interest in electrical energy storage devices but suffer from the risk of thermal runaway, especially under harsh conditions of high temperature or thermal abuse. Pursuing intrinsically thermally stable electrolytes with higher performance and higher safety beyond commercial liquid electrolytes is a major challenge in this field. Here we report on a unique, highly durable sulfolane-based gel electrolyte constructed by a facile gelling strategy. This method takes advantages of thermotolerant sulfolane as a plasticizer and strong dipole-dipole interactions to achieve the gelation of polymer polyvinylidene fluoride/polyethylene oxide. We systematically investigated the influence of gelled sulfolane on gel formation, lithium plating/stripping, and solid electrolyte interphase. Benefiting from favorable interface engineering, the sulfolane-based gel electrolyte remarkably enhances the cyclic and safety performances of LMBs. When used in the Li/$LiCoO_2$ battery, the resulting gel electrolyte enables long-term cycling stability at high temperatures up to 90°C. Moreover, the thermal safety of practical Li/$LiCoO_2$ pouch cells (up to 190°C) has also been demonstrated by accelerating rate calorimetry. These results contribute to the development of high-safety LMBs that require abuse tolerance, high energy, and long calendar life.**

Keywords: lithium-metal batteries, gel electrolytes, solid electrolyte interphases, thermal safety, accelerating rate calorimetry

INTRODUCTION

There has been an ever-increasing demand for lithium-ion batteries (LIBs) with high energy density in areas like electric vehicles, portable electronics, and smart grids during the past few decades [1,2]. Lithium-metal batteries (LMBs) with higher energy density than LIBs have attracted extensive attention [3,4], but suffer from the increased risk of thermal runaway [5,6]. Generally, commercially available carbonate-based electrolytes in LIBs have a great tendency to decompose above 55°C, and the solid electrolyte interphase (SEI) is liable to collapse above 65°C [7–10]. Most carbonate-based electrolytes are volatile and highly flammable, limiting the working temperature of LIBs (<60°C). As for the lithium-metal anode in LMBs, safety issues become severer since lithium is highly reactive with liquid carbonate electrolytes. Meanwhile, parasitic reactions are accelerated, resulting in unstable SEI by consuming more electrolytes and lithium. Eventually, the failure and even thermal runaway of LMBs easily occur at elevated temperatures (>60°C) [3,4,11]. Therefore, it is highly desirable to develop intrinsically thermally stable electrolytes for durable LMBs bearing harsh conditions.

As well known, electrolytes play a vital role in the safety and cyclability of LMBs at elevated temperatures [12–14]. So far, significant advances have been made in liquid electrolytes for LMBs at high temperatures by regulating electrolyte additives, thermally stable solvents, and lithium salts [12–17]. At elevated temperatures, nevertheless, the application of carbonate or ether-based solvents is significantly restricted due to their narrowed electrochemical stability window. Also, their inherent inflammability and volatilization may cause safety concerns. Among various solvents for liquid electrolytes, sulfolane (SL) is well demonstrated to possess a high dielectric constant, wide electrochemical stability window, and low volatility, which holds great promise in safer electrolytes for LMBs requiring thermal and chemical stability [18–20]. However, detrimental side reactions between SL and lithium are inevitable since SL at a high chemical potential state readily reacts with highly active lithium [21,22]. Meanwhile, SL possesses a high viscosity and is poorly wettable toward commercial polyolefin separators. The SL-based localized high-concentration electrolyte was recently reported for LMBs (working below 55°C) to address the interfacial compatibility [21], but little attention was paid to thermal abuse under extreme environments. Besides, it is worth noting that introducing low-boiling-point fluorinated ether would narrow the range of operating temperatures and sacrifice the thermal safety of LMBs [21,23]. Hence, it is significant to fabricate a highly compatible interface between the electrolyte and lithium, which is an essential prerequisite for high-safety and high-durability LMBs under extreme conditions of high temperatures.

In this work, we demonstrate the gelation of liquid SL, including lithium difluoro(oxalate)borate (LiDFOB), within a porous polymer scaffold made of polyvinylidene fluoride/polyethylene oxide (PVDF/PEO). The gel electrolyte/lithium interface could be regulated effectively by the rational design of the SL-gel configuration, taking advantage of strong dipole-dipole interactions. The relationship between SL-derived interfaces and electrochemical properties was systematically explored. It is found that the use of the SL-gel electrolyte contributes to uniform lithium plating/stripping and stable SEI, effectively protecting the metallic lithium anodes and boosting the interfacial compatibility. Furthermore, highly durable SL-gel-based Li/

State Key Laboratory of Materials Processing and Die & Mould Technology, School of Materials Science and Engineering, Huazhong University of Science and Technology, Wuhan 430074, China
* Corresponding author (email: huxl@mail.hust.edu.cn)

$LiCoO_2$ batteries capable of tolerating thermal abuse in a wide temperature range (up to 90°C) have been demonstrated.

EXPERIMENTAL SECTION

Preparation of the porous PVDF/PEO membranes

The porous PVDF/PEO membranes were prepared by a phase-inversion technique. PVDF (Solef 5130) and PEO (M_w: ~1,000,000, Aladdin) were dissolved in a mixture of *N*,*N*-dimethylformamide (DMF, Aladdin, AR) and glycerol (Aladdin, 99%, AR). The weight ratio of PVDF/PEO, glycerol, and DMF was 1:1:10. The porous membranes with different PEO contents were prepared by regulating the PVDF/PEO proportion. After being vigorously stirred for 12 h at 80°C, the homogeneous solutions were cast on a glass plate with a doctor blade, and then placed in an oven at 80°C for 6 h. Finally, white porous PVDF/PEO membranes were obtained by further drying in a vacuum oven at 100°C for 24 h to remove the remaining glycerol. The membranes were made into a wafer with a diameter of 16 mm and a thickness of about 50 μm.

Preparation of SL-gel electrolyte

The 1 mol kg^{-1} SL (99%, Alfa)-based electrolytes were obtained by dissolving the LiDFOB (99.5%, Huizhou Dado New Material Technology Co., Ltd.) salts into the SL solvent with the desired concentration ratios in an Ar-filled glovebox (O_2 < 0.1 ppm, H_2O < 0.1 ppm). The SL solvent was dried with a molecular sieve before use. The obtained porous PVDF/PEO membranes were swelled by 1 mol kg^{-1} SL-based liquid electrolyte for 24 h in an Ar-filled glove box to form the aimed gel electrolyte. The excess liquid electrolyte on the membrane surface was removed by sulfate paper before use.

Electrochemical measurements

The slurry for the $LiCoO_2$ cathode using *N*-methyl-2-pyrrolidinone (NMP, Sigma-Aldrich) as a solvent was coated on a carbon-coated aluminum foil. The dry cathode was composed of 90 wt% $LiCoO_2$, 5 wt% polyvinylidene fluoride binder, and 5 wt% conductive carbon black. The mass loadings of the active material of 5 and 10 mg cm^{-2} were used for the following tests. Electrochemical analysis of the Li/Cu and Li/$LiCoO_2$ cells with the prepared SL-gel electrolyte and SL-based liquid electrolyte was performed in CR2032-type coin cells. The PVDF microporous membrane was used as a separator for the SL-based liquid electrolyte. The electrochemical tests were performed using a coin-type cell (CR2032). Liner sweep voltammetry (LSV), cyclic voltammetry (CV) and electrochemical impedance spectroscopy (EIS) were tested on a CHI 660C electrochemical workstation (ChenHua, Shanghai, China). LSV and CV curves were obtained at a scan rate of 0.5 mV s^{-1}. A Neware battery test system (Neware Technology Co.) and Land test system (Land Electronic Co.) were used for the cycling performance measurements. The Coulombic efficiency (CE) of Li plating/stripping was tested and calculated using the Li/Cu cells with the similar protocol reported before [24].

Materials characterization

Scanning electron microscopy (SEM, HITACHI, SU3500) was adopted to analyze the morphology of the prepared microporous membranes and gel electrolytes. X-ray diffraction (XRD, PANalytical B.V., Holland) and attenuated total refraction Fourier-transform infrared (ATR-FTIR, Bruker Invenio-r) spectroscopy were carried out for the polymer-solvent interaction analysis. The morphologies associated with Li (deposited Li on the cooper and cycled Li anode) were analyzed by SEM (Quanta650 FEG, FEI). X-ray photoelectron spectroscopy (XPS, Thermo Scientific K-Alpha) was used to identify the SEI composition on the cycled Li anode. For the sample preparation, the surface of the deposited Li on copper and the cycled Li anode were cleaned by a pure dimethyl carbonate (DMC) solvent and then dried at 50°C overnight. The samples for XPS characterizations were protected from air and moved to the detector cavity by the transfer equipment filled with high-purity argon gas provided by the Shiyanjia Lab (www.shiyanjia.com). The safety performance of pouch cells was quantified by an accelerating rate calorimeter (BAC-90A, Young instrument) with a typical "heat-wait-seek (HWS)" mode. A 40 mm × 50 mm single-sheet-type pouch cell was fabricated for the accelerating rate calorimetry (ARC) test. The electrodes and SL-gel electrolyte membranes were stacked and packed into a laminate pouch bag. After applying a vacuum to the laminate bag, it was sealed and the pouch cell was obtained. The assembly process was performed in an Ar-filled glovebox.

RESULTS AND DISCUSSION

Two main steps were included in the preparation of SL-based polymer gel electrolytes. Initially, a porous PVDF/PEO membrane of ~50 μm in thickness was prepared through a simple phase-inversion [25,26]. As shown in the SEM image (Fig. 1a), a large number of pores ranging from 150 to 700 nm are present in the PVDF/PEO polymer. After introducing the liquid electrolyte of SL/LiDFOB, the phase state signally evolved from the white solid to transparent gel morphology, achieving the SL-gel electrolyte (Fig. 1b). The gel formation is also confirmed by the XRD, where the two characteristic diffraction peaks for crystalline PEO disappear evidently in the product of SL-gel PVDF/PEO (Fig. S1). By comparing the liquid uptake and lithium-ion conductivity of the SL-gel PVDF/PEO membranes with different PVDF/PEO mass ratios, it is determined that the SL-gel electrolyte derived from the PVDF/PEO membrane with a mass ratio of 8:2 has the highest lithium-ion conductivity (Fig. S2). The ionic conductivity of the designed gel electrolyte is optimized to be 1.85×10^{-3} S cm^{-1} at 90°C. It has been previously reported that polar polymer-solvent interactions could inhibit side reactions between the corrosive electrolyte and lithium [27]. As expected (Fig. 1c), gelling SL and introducing strong dipole-dipole interactions may also stabilize the SL plasticizer within PVDF/PEO, thus boosting uniform lithium plating/stripping and robust SEI during continuous cycles. In contrast, free SL molecules in the liquid electrolyte of SL/LiDFOB react readily with lithium, causing the growth of lithium dendrites and unstable SEI (Fig. 1d). As for the SL-gel PVDF/PEO electrolyte, it is compatible with lithium and enhances the redox stability of SL molecules. On the one hand, PVDF with high thermal stability and excellent solvent resistance functions as the stable skeleton (Fig. S3). On the other hand, polar PEO serving as the semi-interpenetrating network offers many oxygen-containing bonds capable of anchoring polar SL molecules (Fig. 1c) through dipole-dipole interactions. As a result, the local Li^+ solvation environment and chemical potential of SL molecules due to the PEO-SL interaction are correspondingly altered towards preferable compatibility with lithium.

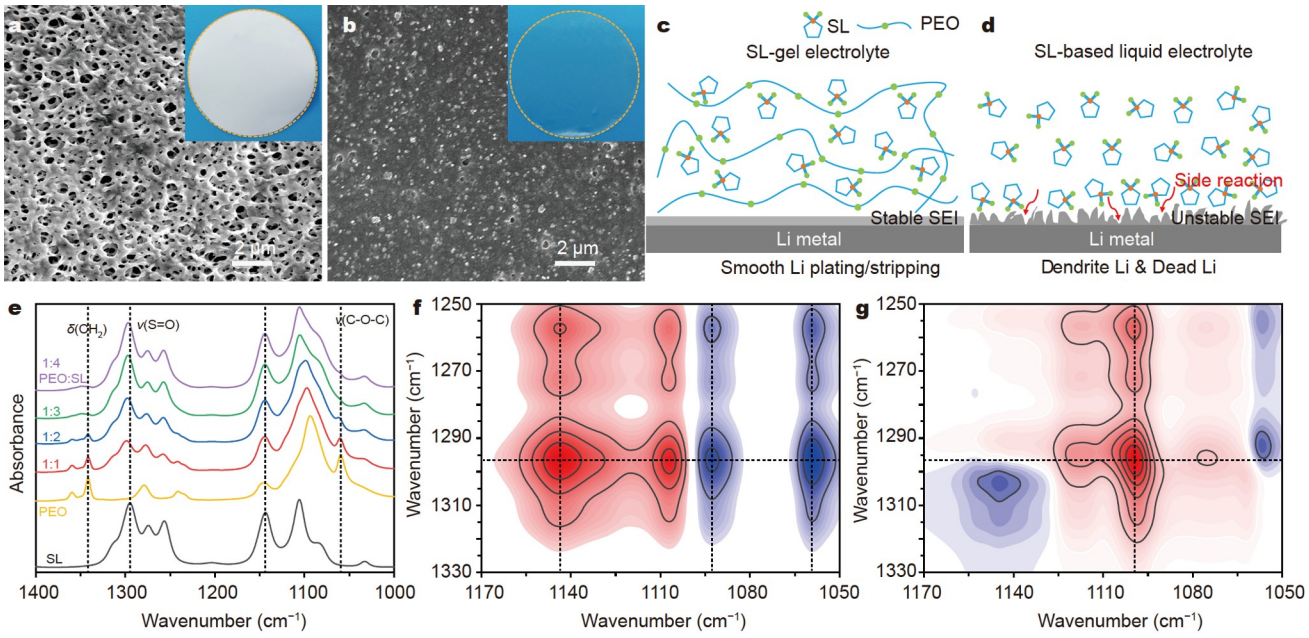

Figure 1 SEM images of the PVDF/PEO framework (a) before and (b) after swelling SL/LiDFOB (insets: corresponding digital photos). (c, d) Schematic illustration of PEO-SL interaction improving the compatibility between the SL-based liquid electrolyte and lithium metal. (e) ATR-FTIR spectra of PEO, SL, and PEO/SL with different mass ratios. (f) Synchronous and (g) asynchronous 2D correlation contour maps of concentration-dependent FTIR spectra for PEO/SL according to the bands for S=O (ordinate) and C–O–C (abscissa).

Fig. 1e displays the ATR-FTIR spectra in the 1400–1000 cm^{-1} region for PEO, SL and PEO/SL blends. The characteristic C–O–C stretching bands for PEO at 1059.7 cm^{-1} and S=O stretching vibrations for SL at 1294.9 cm^{-1} show pronounced shift upon increasing the SL amount, indicative of the typical PEO-SL interaction [28]. However, it is noted that the position shift for CH_2 bending and wagging (1341.5 and 1359.5 cm^{-1}, crystalline phase) of PEO was not detectable with the increase of SL. These FTIR results indicate that the PEO-SL interaction occurs between dipole-dipole C–O–C and S=O groups, instead of CH_2 groups. The PEO-SL interaction was further verified by two-dimensional (2D) correlation spectroscopy constructed from the SL-dependent FTIR spectra of the PEO/SL blends. Fig. 1f, g depict synchronous and asynchronous correlation contour maps based on the stretching region of S=O and C–O–C groups, respectively. The peak intensity at 1296.9 cm^{-1} exhibits intensive positive correlations to those at 1092.9 and 1143.6 cm^{-1} (Fig. 1f). Also, positive correlations are observable between the bands at 1296.9 and 1099.7 cm^{-1} in the asynchronous 2D correlation spectrum (Fig. 1g). These autopeaks in the 2D correlation spectra further confirm the dipole-dipole interaction among the C–O–C and S=O groups [29].

Furthermore, the effect of the PEO-SL interaction on the redox stability of SL at 30 and 90°C was directly evidenced by CV and LSV. Fig. 2a shows the initial CV curves for the SL/LiDFOB liquid electrolyte and SL-based gel electrolyte in the potential range of 0–2.5 V at 90°C. Both samples exhibit an intensive peak at ~1.75 V, which corresponds to the reduction reaction of $DFOB^-$ anions [30,31]. Besides, two pronounced reduction peaks arising from the SL decomposition appear at lower potentials of 0.65 and 1.20 V for the SL/LiDFOB liquid electrolyte [22]. Compared with SL in the liquid electrolyte, no prominent peaks for reducing SL in the gel electrolyte were observed at 90°C, suggesting enhanced reduction stability of gelled SL based on the PEO-SL interaction. The results at 30°C suggest the enhanced reduction stability of the gelled SL (Fig. S4a). The LSV results also confirm the outstanding oxidation stability and wide electrochemical stability window (>4.7 V) of the SL-gel electrolyte, even at elevated temperatures up to 90°C (Fig. 2b and Fig. S4b). From the direct-current (DC) polarization results of the Li/SL-gel/Li symmetrical batteries, the lithium-ion transference number of the SL-gel electrolyte is calculated to be 0.368 at 30°C and 0.355 at 90°C (Fig. S5). The similar lithium-ion transference numbers for the SL-gel electrolytes at 30 and 90°C further prove the excellent stability of the SL-gel electrolyte. Representative mechanical properties of the PVDF/PEO membrane and the SL-gel electrolyte were determined by stress-strain measurements (Fig. S6). The yield strength and elongation at break of the SL-gel electrolyte can still reach 3.1 MPa and 49.0%, respectively.

To further verify the potential of the SL-gel electrolyte in the practical application of LMBs, Li/$LiCoO_2$ full cells in a wide temperature range between 30 and 90°C were investigated. The cyclability of Li/$LiCoO_2$ cells was evaluated at 1 C between 3.0 and 4.2 V after activation at 0.1 C for two cycles. As shown in Fig. 2c, d, the Li/SL-gel/$LiCoO_2$ cell demonstrates an outstanding cyclability with capacity retention of 92.3% after 150 cycles and overall CE up to 99.5% at 30°C (Fig. 2c). When the operating temperature increases to 90°C, the Li/SL-gel/$LiCoO_2$ cell exhibits a high initial discharge capacity of 144.6 mA h g^{-1} at 1 C and retains 135.1 mA h g^{-1} even after 150 cycles, and capacity retention of 93.4% with an average CE up to 99.4% after 150 cycles is achieved (Fig. 2d, e). In contrast, the Li/$LiCoO_2$ battery with the SL-based liquid electrolyte could be reversibly charged and discharged for less than 10 cycles at 30 and 90°C. An obvious overcharge appears in the subsequent cycles with low CEs (Fig. 2f). The failure may arise from the local micro short circuit inside the battery caused by the growth of lithium den-

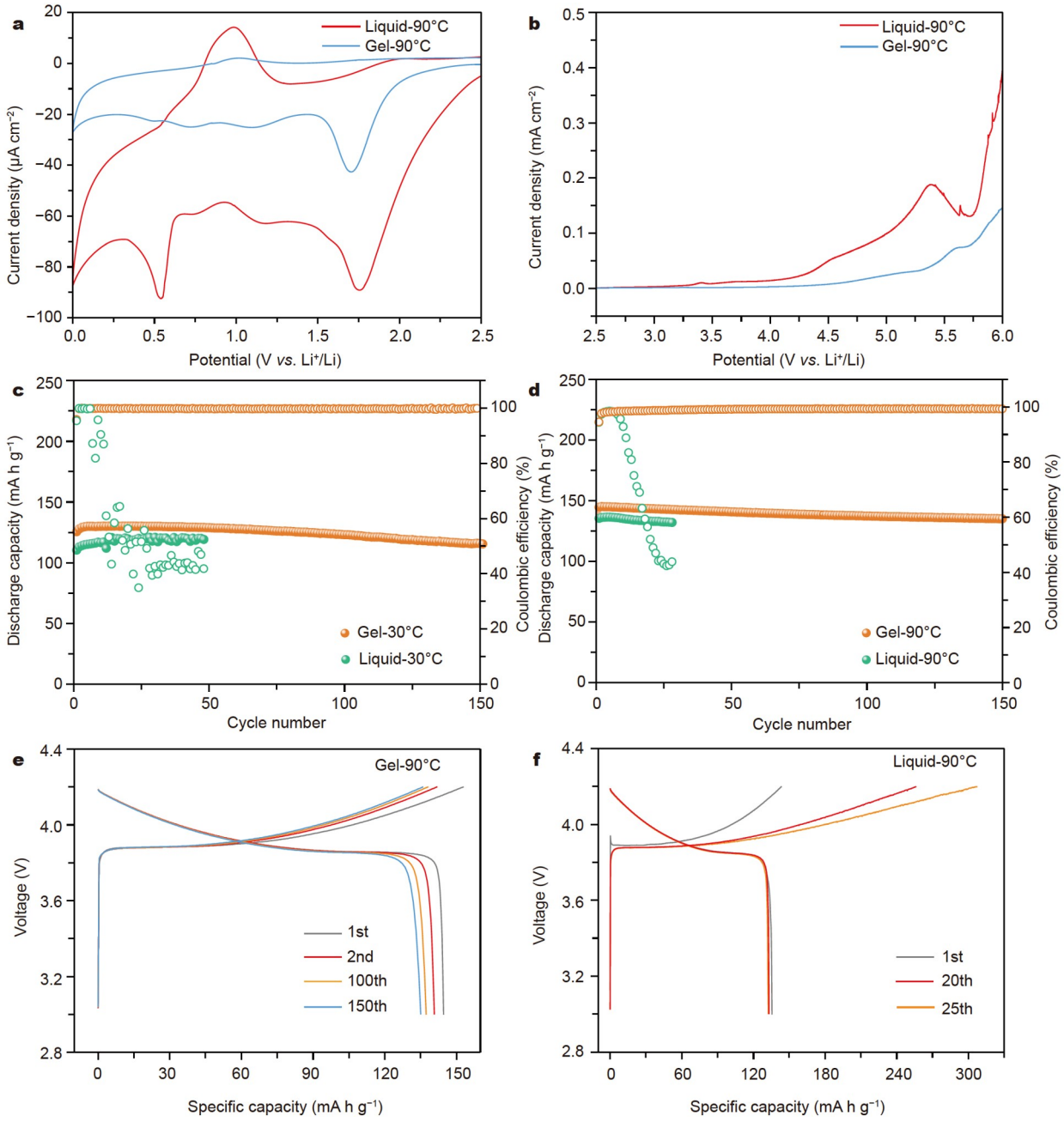

Figure 2 (a) Initial CV curves for the SL-gel electrolyte and SL-based liquid electrolyte in the potential range of 0–2.5 V at a scanning rate of 0.5 mV s^{-1} at 90°C. (b) LSV curves for the SL-gel electrolyte and SL-based liquid electrolyte in the potential range of 2.5–6.0 V at a scanning rate of 0.5 mV s^{-1} at 90°C. Cycling performances of the Li/$LiCoO_2$ batteries with the SL-gel electrolyte and SL-based liquid electrolyte at (c) 30°C and (d) 90°C. Galvanostatic charge/discharge curves of Li/$LiCoO_2$ batteries with (e) the SL-gel electrolyte and (f) the SL-based liquid electrolyte at 90°C (mass loading in the cathode: 5 mg cm^{-2}; 1 C = 140 mA h g^{-1}).

drites penetrating the separator. When the active mass loading in the cathode was improved to 10 mg cm^{-2}, the Li/SL-gel/$LiCoO_2$ battery could still achieve a 94% capacity retention upon 100 cycles at 0.5 C and 90°C (Fig. S7). A high discharge capacity of 120 mA h g^{-1} is also achieved at a high current density of 2 C (2.8 mA cm^{-2}). However, the high-mass-loading Li/$LiCoO_2$ battery based on the SL-based liquid electrolyte can only survive at 0.2 C with slight overcharge and low CE (Fig. S8). Evidently, severe overcharge occurred at 0.5 C (Figs S7d and S8). These results demonstrate that the SL-gel electrolyte boosts stable cycling of Li/$LiCoO_2$ LMBs in a wide temperature range from 30 to 90°C and overcomes the upper limit of operating temperature for traditional LIBs (usually 55–60°C). Therefore, the risk of thermal runaway would be effectively reduced, and the thermal management system of LMBs in reality could be simplified.

ARC measurements were performed to evaluate the thermal safety of the Li/$LiCoO_2$ pouch cells based on different electrolytes. As shown in Fig. 3a, the full-charged Li/SL-gel/$LiCoO_2$ pouch cell exhibits the typical onset temperature of thermal runaway at 190°C, higher than that (130°C) of the Li/$LiCoO_2$ cell using a commercially available liquid electrolyte containing $LiPF_6$, ethylene carbonate (EC), DMC and ethyl methyl carbo-

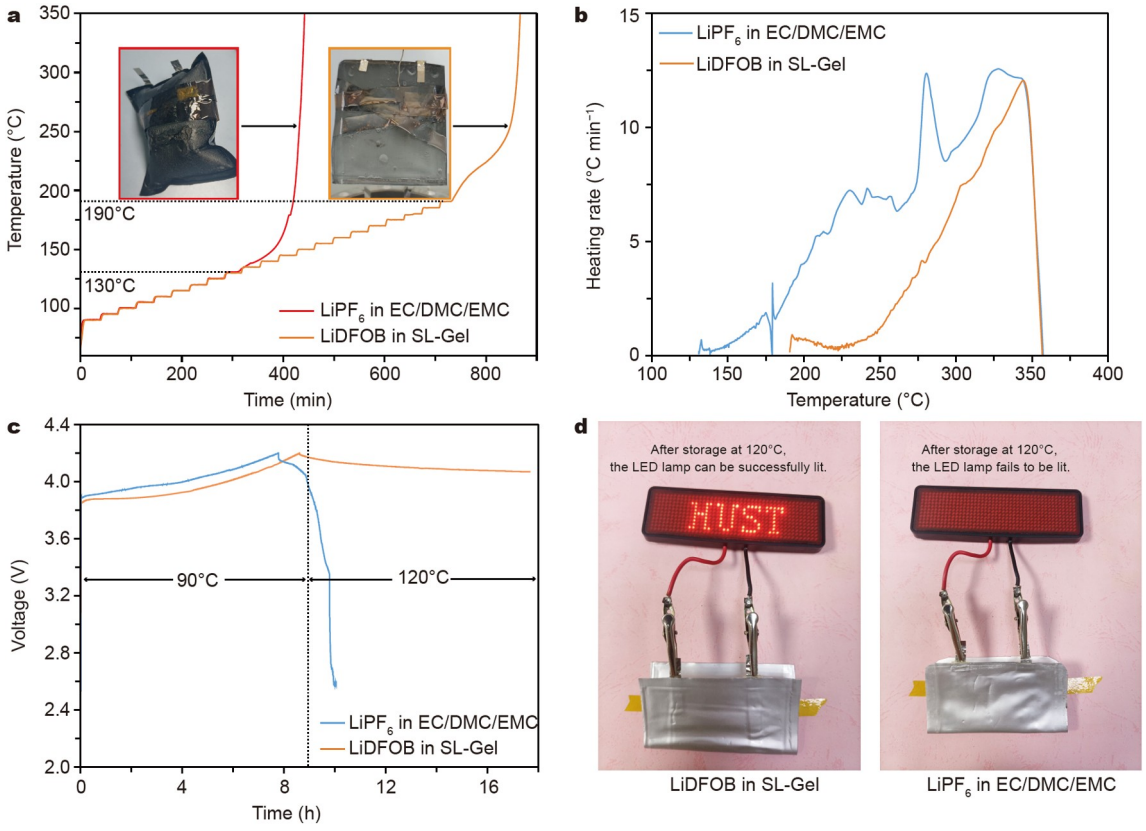

Figure 3 (a) ARC results of Li/$LiCoO_2$ pouch cells with the SL-gel electrolyte and commercial carbonate electrolyte (inset: corresponding digital photos of pouch cells after the simulated thermal runaway). (b) Self-heating rate *versus* temperature for the Li/$LiCoO_2$ pouch cells with different electrolytes. (c) Voltage profiles of the full-charged Li/$LiCoO_2$ pouch cells (initially charged to 4.2 V at 90°C) with different electrolytes against the storage time at 120°C. (d) Comparison of the powering ability of the Li/$LiCoO_2$ pouch cells with different electrolytes after being stored at a high temperature of 120°C for 8 h.

nate (EMC). Moreover, the self-heating rate of the Li/SL-gel/$LiCoO_2$ pouch cell upon heating is much lower than that of the Li/$LiCoO_2$ pouch cell using the liquid electrolyte (Fig. 3b). After ARC tests, the volume swelling for the Li/SL-gel/$LiCoO_2$ pouch cell is negligible, whereas the liquid-electrolyte-based Li/$LiCoO_2$ pouch cell is visibly expanded (inset of Fig. 3a). These ARC results further confirm the superior thermal safety of the Li/$LiCoO_2$ pouch cell using the SL-gel electrolyte. Upon storage at a harsh condition of high temperature at 120°C for 8 h, the full-charged Li/SL-gel/$LiCoO_2$ pouch cell could still maintain the voltage stability and light up the light emitting diode (LED) lamp (Fig. 3c, d). Instead, the failure for Li/$LiCoO_2$ pouch cell with the liquid electrolyte quickly happened at 120°C.

To gain a more insightful understanding, we have further explored the morphology of lithium-metal anodes in Li/$LiCoO_2$ batteries (cathode loading: 10 mg cm^{-2}) after 100 cycles at 90°C. Owing to the continuous side reaction between the SL-based liquid electrolyte and lithium, a large number of corroded holes appear on the surface of the cycled lithium foil at 90°C (Fig. S9a). In addition, the cross-section SEM image shows significant deterioration of the bulk lithium metal (Fig. S9b), where a loose dead lithium layer of ~50 μm in thickness is generated after 100 cycles at 90°C. The as-formed loose dead lithium layer adheres easily to the separator and grows along the pores within the separator (Fig. S10a), and the dead lithium on the separator is also loosely porous (Fig. S10b). In comparison, the cycled lithium anode at 90°C from the SL-gel-based battery exhibits a smooth surface upon 100 cycles, and the accumulation of dead lithium is absent (Figs S9c, d and S10c). The above results confirm that the SL-gel electrolyte plays a crucial role in suppressing side reactions with the lithium anode at 90°C. For the SL-based liquid electrolyte, abundant free SL molecules on the exposed surface of the lithium anode are vulnerable to react with lithium, resulting in unstable SEI. Meanwhile, lithium dendrites continuously grow and accumulate, which eventually induces battery failure, especially at elevated temperatures.

As shown in Fig. 4a, the lithium plating/stripping behavior of the Li/SL-gel/Cu battery (areal capacity: 2 mA h cm^{-2}) shows excellent stability with a high average CE of 98.2% at 90°C. However, for the Li/Cu battery with the SL-based liquid electrolyte, a significantly increased polarization appears during the long-term plating/stripping process, and the short circuit occurs after 80 cycles (Fig. 4b), mainly arising from the dendrite growth and accumulation of dead lithium due to the continuous side reactions in the liquid electrolyte at 90°C. The SL-gel electrolyte can maintain good stability to achieve a stable and efficient lithium plating/stripping at 90°C. SEM morphologies of the deposited lithium (0.5 mA cm^{-2}; 4 mA h cm^{-2}) at different temperatures are displayed in Fig. 4c–h. The deposited lithium with the SL-gel electrolyte presents a dendrite-free and compact lithium surface (Fig. 4c–e). In comparison, microsized lithium dendrites are present for the battery with the SL-based liquid electrolyte, and the surface of the deposited lithium is rough and porous (Fig. 4f–h). The size of the lithium nuclei increases remarkably with the increase of temperature due to the enhanced lithiophilicity and Li-ion mobility at elevated tem-

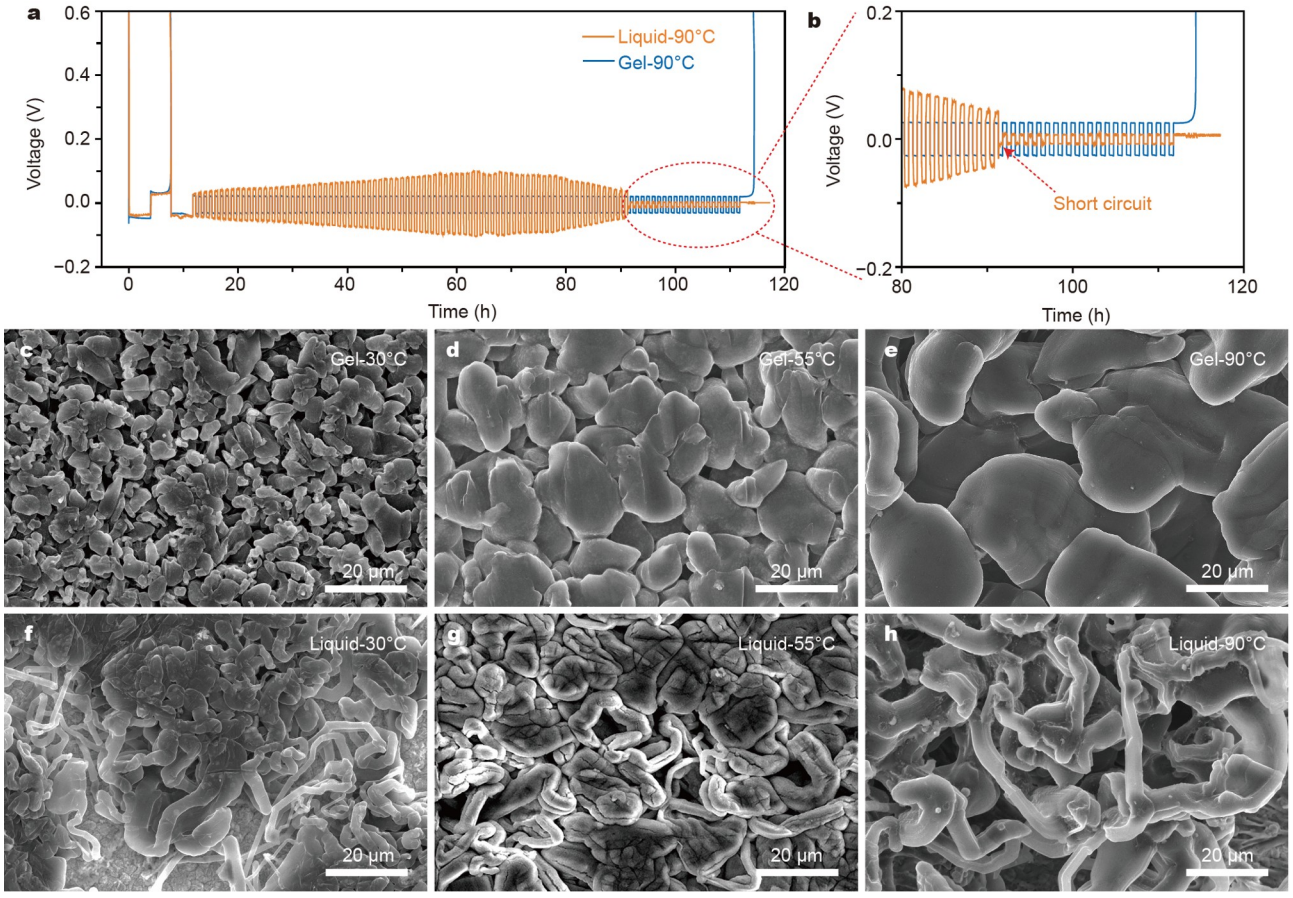

Figure 4 (a) Lithium plating/stripping profiles for lithium metal on a Cu foil with SL-gel electrolyte and SL-based liquid electrolyte at 0.5 mA cm^{-2} and 0.25 mA h cm^{-2} for 100 cycles at 90°C. (b) Enlarged profiles from (a). SEM images of the deposited lithium with (c–e) SL-gel electrolyte and (f–h) SL-based liquid electrolyte at different temperatures (30, 55, and 90°C).

peratures [32].

The high CE and excellent cyclability of the SL-gel electrolyte at elevated temperatures agree well with the uniform morphology of lithium deposition. The severe growth of lithium dendrites at elevated temperatures with the SL-based liquid electrolyte brings about a noticeable short circuit. The lithium dendrites may penetrate the separator, causing thermal runaway or even explosion of batteries. Energy-dispersive X-ray spectroscopy (EDS) mapping was conducted to explore the distinguished lithium plating/stripping behavior with the SL-gel electrolyte and SL-based liquid electrolyte at 90°C (Fig. S11). Compared with the SL-gel electrolyte, the signal for the S element of the SL-based liquid electrolyte is not uniform and mainly appears in the regions of uneven lithium deposition. Furthermore, the S amount on the surface of deposited lithium with the SL-based liquid electrolyte is much higher than that of the SL-gel electrolyte at 90°C (Fig. S12). The uneven lithium deposition and dendrite growth with the SL-based liquid electrolyte at 90°C result from the decomposition of the liquid electrolyte, which is effectively inhibited by the SL-gel electrolyte benefiting from the polar polymer-solvent interaction. Therefore, it is confirmed that the SL-gel electrolyte facilitates the excellent stability of lithium plating/stripping at 90°C.

The chemical composition of the SEI layer generated on the cycled lithium anode at 90°C using different electrolytes was further investigated by XPS. The C 1s XPS spectra for the SEI compositions on the surface of the cycled lithium-metal anode with the SL-gel electrolyte and SL-based liquid electrolyte are similar (Fig. 5a, b). The C–C/C–H (~284.7 eV), C–O/C–S (~286.3 eV), and C=O/C–SO_x (~288.7 eV) peaks are derived from the reduction products of LiDFOB and SL [21,22,33]. The proportion of C–S and C–SO_x components attributed to the decomposition of SL in the SL-gel electrolyte is much smaller than that of the liquid electrolyte, suggesting that the decomposition reaction of SL molecules in the gel electrolyte is greatly inhibited at 90°C. In addition, the peaks for C 1s of the dead lithium layer indicate that the decomposition of SL molecules in the liquid electrolyte occurs more easily at 90°C (Fig. 5c). As expected for the electrochemical decomposition from the fluorine-containing $DFOB^-$ anions, the F 1s peaks corresponding to LiF (~684.5 eV) were observed (Fig. 5d–f) [34,35]. The decomposition of $DFOB^-$ in the SL-gel electrolyte is sufficient to produce more LiF, while the liquid electrolyte still contains a large part of insufficiently decomposed B–F components, especially in the dead lithium layer. The SEI compositions for different electrolytes were further studied by Ar^+ sputtering for 50 nm at an etching rate of 0.2 nm s^{-1}. The change of the C 1s and F 1s peaks for the SL-gel electrolyte is hardly observed with the etch proceeding, indicating the homogeneous distribution of SEI. In comparison, the uneven distribution of SEI components for the liquid electrolyte appears after etching. The enhanced intensity of the LiF peaks for the liquid electrolyte after etching

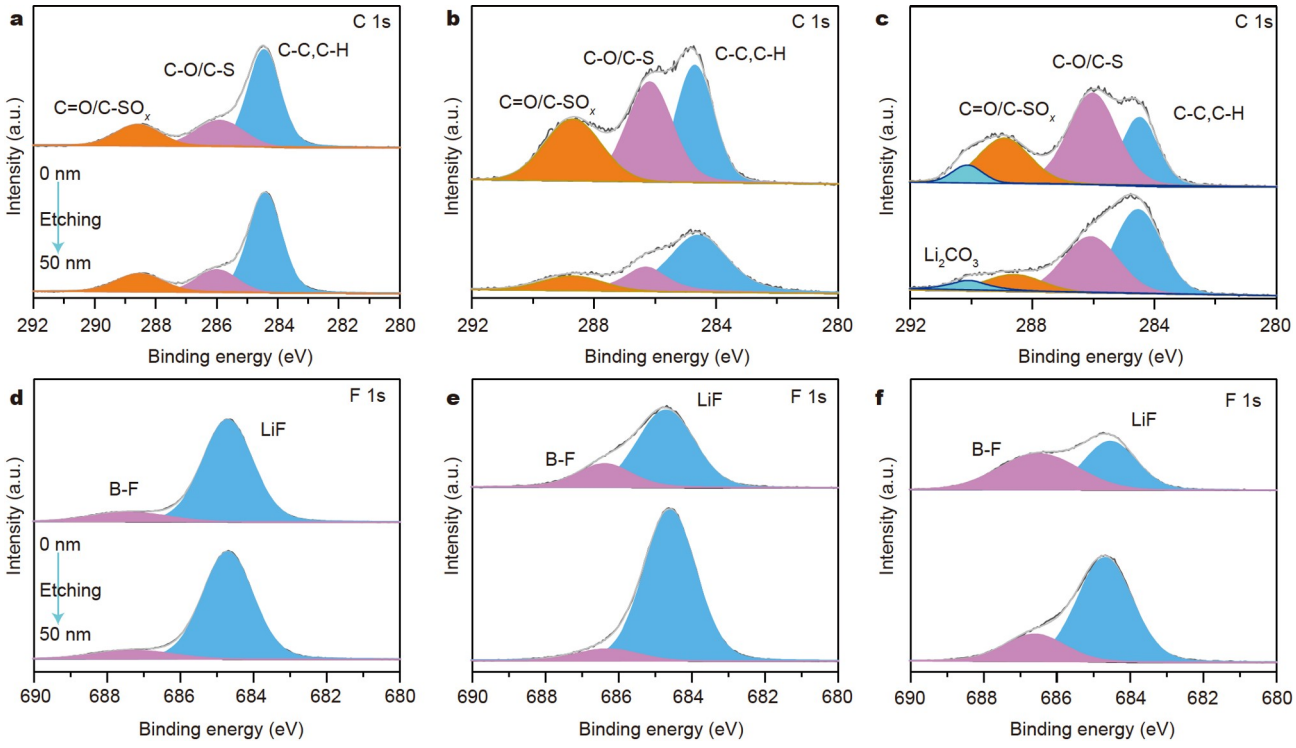

Figure 5 XPS spectra for C 1s and F 1s of the lithium anode after 100 cycles at 90°C using different electrolytes: (a, d) SL-gel electrolyte; (b, e) SL-based liquid electrolyte. (c, f) XPS spectra for C 1s and F 1s of the dead lithium attached to the separator after 100 cycles at 90°C using the SL-based liquid electrolyte. The lithium anode was from the Li/$LiCoO_2$ batteries upon 100 cycles at 0.5 C.

can be assigned to the continuous decomposition of the electrolyte, thus leading to continuous accumulation in the inner layer. Also, the accumulation of dead lithium layers in the SL-based liquid electrolyte arises from the continuous decomposition of the solvent and lithium salts upon charge/discharge cycles. Therefore, uniform lithium deposition based on the SL-gel electrolyte at 90°C is beneficial to forming a more robust and stable SEI and preventing other side reactions between the electrolyte and lithium metal.

CONCLUSIONS

In conclusion, we have successfully demonstrated the design and fabrication of an SL-gel electrolyte that is compatible with the lithium anode and enables stable SEI for constructing durable and safe Li/$LiCoO_2$ batteries. Such a unique SL-gel electrolyte exhibits high redox stability in a wide temperature range, benefiting from the strong dipole-dipole interactions among polar SL molecules and the PEO matrix. As demonstrated, the SL-gel-based Li/$LiCoO_2$ full cells could be stably cycled at 90°C over 150 cycles with a capacity retention of 93.4%. Furthermore, thermal safety till 190°C of the Li/$LiCoO_2$ pouch cell monitored by ARC is verified under simulated thermal-runaway conditions. This work provides a promising interface engineering strategy for developing high-performance gel electrolytes for advanced safe LMBs, reducing the risk of thermal runaway under temperature extremes.

Received 8 February 2022; accepted 29 April 2022; published online 19 July 2022

1 Bresser D, Hosoi K, Howell D, *et al.* Perspectives of automotive battery R&D in China, Germany, Japan, and the USA. J Power Sources, 2018, 382: 176–178
2 Li H. Practical evaluation of Li-ion batteries. Joule, 2019, 3: 911–914
3 Cheng XB, Zhang R, Zhao CZ, *et al.* Toward safe lithium metal anode in rechargeable batteries: A review. Chem Rev, 2017, 117: 10403–10473
4 Tarascon JM, Armand M. Issues and challenges facing rechargeable lithium batteries. Nature, 2001, 414: 359–367
5 Liu H, Wei Z, He W, *et al.* Thermal issues about Li-ion batteries and recent progress in battery thermal management systems: A review. Energy Convers Manage, 2017, 150: 304–330
6 Wang L, Zhou Z, Yan X, *et al.* Engineering of lithium-metal anodes towards a safe and stable battery. Energy Storage Mater, 2018, 14: 22–48
7 Campion CL, Li W, Lucht BL. Thermal decomposition of $LiPF_6$-based electrolytes for lithium-ion batteries. J Electrochem Soc, 2005, 152: A2327
8 Zu C, Yu H, Li H. Enabling the thermal stability of solid electrolyte interphase in Li-ion battery. InfoMat, 2021, 3: 648–661
9 Koch S, Fill A, Birke KP. Comprehensive gas analysis on large scale automotive lithium-ion cells in thermal runaway. J Power Sources, 2018, 398: 106–112
10 Wang Q, Sun J, Yao X, *et al.* Thermal behavior of lithiated graphite with electrolyte in lithium-ion batteries. J Electrochem Soc, 2005, 153: A329
11 Wu Y, Wang S, Li H, *et al.* Progress in thermal stability of all-solid-state-Li-ion-batteries. InfoMat, 2021, 3: 827–853
12 Hou LP, Zhang XQ, Li BQ, *et al.* Cycling a lithium metal anode at 90 °C in a liquid electrolyte. Angew Chem Int Ed, 2020, 132: 15221–15225
13 Hou J, Yang M, Wang D, *et al.* Fundamentals and challenges of lithium ion batteries at temperatures between −40 and 60 °C. Adv Energy Mater, 2020, 10: 1904152
14 Geng Z, Lu J, Li Q, *et al.* Lithium metal batteries capable of stable operation at elevated temperature. Energy Storage Mater, 2019, 23: 646–652
15 Yang H, Guo C, Chen J, *et al.* An intrinsic flame-retardant organic electrolyte for safe lithium-sulfur batteries. Angew Chem Int Ed, 2019,

58: 791–795
16 Xu C, Hernández G, Abbrent S, *et al.* Unraveling and mitigating the storage instability of fluoroethylene carbonate-containing $LiPF_6$ electrolytes to stabilize lithium metal anodes for high-temperature rechargeable batteries. ACS Appl Energy Mater, 2019, 2: 4925–4935
17 Wang J, Yamada Y, Sodeyama K, *et al.* Fire-extinguishing organic electrolytes for safe batteries. Nat Energy, 2018, 3: 22–29
18 Alvarado J, Schroeder MA, Zhang M, *et al.* A carbonate-free, sulfone-based electrolyte for high-voltage Li-ion batteries. Mater Today, 2018, 21: 341–353
19 Xu K. Electrolytes and interphases in Li-ion batteries and beyond. Chem Rev, 2014, 114: 11503–11618
20 Tong B, Song Z, Wan H, *et al.* Sulfur-containing compounds as electrolyte additives for lithium-ion batteries. InfoMat, 2021, 3: 1364–1392
21 Ren X, Chen S, Lee H, *et al.* Localized high-concentration sulfone electrolytes for high-efficiency lithium-metal batteries. Chem, 2018, 4: 1877–1892
22 Fu J, Ji X, Chen J, *et al.* Lithium nitrate regulated sulfone electrolytes for lithium metal batteries. Angew Chem Int Ed, 2020, 132: 22378–22385
23 Cao X, Jia H, Xu W, *et al.* Review—Localized high-concentration electrolytes for lithium batteries. J Electrochem Soc, 2021, 168: 010522
24 Adams BD, Zheng J, Ren X, *et al.* Accurate determination of coulombic efficiency for lithium metal anodes and lithium metal batteries. Adv Energy Mater, 2018, 8: 1702097
25 Li J, Xi J, Song Q, *et al.* Microporous polymer electrolyte based on PVDF-PEO. Chin Sci Bull, 2005, 50: 368–370
26 Xi J, Qiu X, Li J, *et al.* PVDF-PEO blends based microporous polymer electrolyte: Effect of PEO on pore configurations and ionic conductivity. J Power Sources, 2006, 157: 501–506
27 Bae J, Qian Y, Li Y, *et al.* Polar polymer-solvent interaction derived favorable interphase for stable lithium metal batteries. Energy Environ Sci, 2019, 12: 3319–3327
28 Dhatarwal P, Sengwa RJ. Polymer compositional ratio-dependent morphology, crystallinity, dielectric dispersion, structural dynamics, and electrical conductivity of PVDF/PEO blend films. Macromol Res, 2019, 27: 1009–1023
29 Wu QY, Chen XN, Wan LS, *et al.* Interactions between polyacrylonitrile and solvents: Density functional theory study and two-dimensional infrared correlation analysis. J Phys Chem B, 2012, 116: 8321–8330
30 Shkrob IA, Zhu Y, Marin TW, *et al.* Mechanistic insight into the protective action of bis(oxalato)borate and difluoro(oxalate)borate anions in Li-ion batteries.. J Phys Chem C, 2013, 117: 23750–23756
31 Rodrigo ND, Tan S, Shadike Z, *et al.* Improved low temperature performance of graphite/Li cells using isoxazole as a novel cosolvent in electrolytes. J Electrochem Soc, 2021, 168: 070527
32 Yan K, Wang J, Zhao S, *et al.* Temperature-dependent nucleation and growth of dendrite-free lithium metal anodes. Angew Chem Int Ed, 2019, 131: 11486–11490
33 Lu D, Xu G, Hu Z, *et al.* Deciphering the interface of a high-voltage (5 V-class) Li-ion battery containing additive-assisted sulfolane-based electrolyte. Small Methods, 2019, 3: 1900546
34 Sun HH, Dolocan A, Weeks JA, *et al. In situ* formation of a multi-component inorganic-rich SEI layer provides a fast charging and high specific energy Li-metal battery. J Mater Chem A, 2019, 7: 17782–17789
35 Jurng S, Brown ZL, Kim J, *et al.* Effect of electrolyte on the nanostructure of the solid electrolyte interphase (SEI) and performance of lithium metal anodes. Energy Environ Sci, 2018, 11: 2600–2608

Acknowledgements This work was financially supported by the National Natural Science Foundation of China (51972132 and 51772116), and the Program for Huazhong University of Science and Technology Academic Frontier Youth Team (HUST, 2016QYTD04). The authors thank the Analytical and Testing Center of HUST for the FTIR, XRD and SEM measurements.

Author contributions Hu X conceived the idea of this work and revised the manuscript; Yu X conducted the experiments and data analysis and wrote the manuscript. All authors contributed to the general discussion.

Conflict of interest The authors declare that they have no conflict of interest.

Supplementary information Supporting data are available in the online version of the paper.

Xinrun Yu is currently a PhD candidate at the School of Materials Science and Engineering, Huazhong University of Science and Technology (HUST) under the supervision of Prof. Xianluo Hu. His research interests focus on advanced electrolytes for high-temperature electrochemical energy storage devices.

Xianluo Hu is a full professor of materials science and engineering at HUST. He received his PhD degree from the Chinese University of Hong Kong (CUHK) in 2007 and subsequently worked as a postdoctoral researcher at CUHK and a JSPS (Japan Society for the Promotion of Science) postdoctoral fellow at the National Institute of Materials Science (NIMS) of Japan from 2007 to 2009. His current research interests focus on safe lithium batteries under extreme conditions.

环丁砜凝胶化界面工程助力安全耐用的宽温域 Li/$LiCoO_2$电池

虞鑫润, 胡先罗*

摘要 高能量密度锂金属电池在电化学储能领域受到了广泛关注, 但其存在热失控的风险. 尤其在高温或热滥用等恶劣条件下, 安全隐患更加凸显. 研发本征热稳定、高安全电解质是该领域的一个主要挑战. 在该工作中, 我们提出了一种简单易操作的凝胶化策略, 制备出独特的、高热稳定的环丁砜基凝胶电解质. 采用耐高温环丁砜作为增塑剂, 通过强偶极-偶极相互作用, 实现了聚偏氟乙烯/聚环氧乙烷基质之间的凝胶化, 并系统地研究了砜基凝胶对凝胶化过程、锂沉积/剥离和固态电解质界面的影响. 由于良好的界面特性, 砜基凝胶电解质显著提高了锂金属电池的长循环和安全性能. 由凝胶电解质组装的Li/$LiCoO_2$电池, 在高温(高达90°C)条件下仍然呈现出优异的循环稳定性. 此外, 通过加速量热仪证实了Li/$LiCoO_2$软包电池的高热安全性(>190°C). 该研究工作为开发耐滥用、高比能和长寿命的高安全性锂金属电池提供了新方法.

